Violating the Energy-Momentum Proportionality of Photonic Crystals in the Low-Frequency Limit

Michael J. A. Smith[*]

School of Mathematics, The University of Manchester, Manchester M13 9PL, United Kingdom

Parry Y. Chen

Unit of Electro-optic Engineering, Faculty of Engineering Sciences, Ben-Gurion University, Beer Sheva, Israel
School of Physics and Astronomy, Raymond and Beverly Sackler Faculty of Exact Sciences, Tel Aviv University, Tel Aviv, Israel

We theoretically show that the frequency and momentum of a photon are not necessarily proportional to one another at low frequencies in photonic crystals comprising materials with positive- and negative-valued material properties. We rigorously determine closed-form conditions for the light cone to emanate from points other than the origin of k space, ultimately decoupling the first band from the origin and demonstrating light propagation at zero energy with nonzero crystal momentum. We also numerically show that first bands can originate from an arbitrary Bloch coordinate as well as from multiple coordinates simultaneously.

When a photon propagates through a dielectric medium at low frequencies, it satisfies the energy-momentum ($E - k$) relation $E = c\hbar|\mathbf{k}|$, where c is the phase velocity in the medium [1,2]. This relation ensures that at zero energy, the photon possesses zero momentum. Fundamental relations of this type are prevalent throughout nature and are not isolated to photons, e.g., electrons propagate through a crystal lattice as $E = \hbar^2/(2m_{\text{eff}})|\mathbf{k}|^2$ at low energies, where m_{eff} is the effective mass [3]. This proportionality is fundamental for the study of particles and fields in relativistic mechanics, particle physics, and quantum mechanics.

In this Letter, we break the conventional low-frequency $E - k$ proportionality for photons, obtaining relations of the form $E = C|\mathbf{k} - \Xi|$, where Ξ denotes a high-symmetry point of the reciprocal lattice and $\mathbf{k}$ is the crystal momentum [see Figs. 1(a)–1(c)]. This is achieved in two-dimensional photonic crystals comprising materials with *positive-definite* and *negative-definite* [4–6] optical properties. We present explicit conditions on the constituent properties and explicit forms for the proportionality constants C, for all high-symmetry coordinates of a square lattice. Furthermore, we numerically demonstrate the existence of other novel low-frequency behaviors, including photonic crystals with $E = C_1|\mathbf{k}| + C_2|\mathbf{k} - \mathbf{X}|$, where C_j are proportionality constants and X is a high-symmetry point [see Fig. 3(e)]. Such unconventional behavior contrasts the standard outcomes for light in photonic crystals, where either $E - k$ proportionality is supported, or there exists a complete band gap [7], at low frequencies.

In the nonstandard photonic settings we describe, massless photons are predicted to propagate as massive polaritons which travel superfluidically through the medium [8].

Consequently, our findings have the potential to motivate the development of new photonic devices, and to deepen our understanding of light in structured media. The behaviors we describe complement existing observations in optical systems incorporating negative-definite materials, such as folded band surfaces with infinite group velocities [9], cloaking and superresolution [10,11], and new types of band gaps [12]. Analogies to our low-frequency $E - k$ relations may be found in the electronic properties of transition-metal perovskites, where the first band is centered about high symmetry points other than the origin [13,14].

We begin by considering the modes of the time-harmonic form of the source-free Maxwell equations in a nondispersive and lossless system with Bloch vectors $\mathbf{k} = (k_x, k_y, 0)$. This wave vector restriction reduces Maxwell's equations to the Helmholtz equation

$$\nabla_\perp \cdot (\varepsilon_r^{-1}\nabla_\perp H_z) + \omega^2 c_0^{-2}\mu_r H_z = 0, \tag{1}$$

for fields polarized as $\mathbf{H} = (0, 0, H_z)$. Here, $\nabla_\perp \equiv (\partial_x, \partial_y)$, ε_r is the relative permittivity, μ_r the relative permeability, ω the angular frequency, and c_0 is the speed of light in vacuum. We consider an array of infinitely extending isotropic cylinders, periodically positioned in the (x, y) plane at the coordinates of a square lattice, and which are embedded in an infinitely extending isotropic background material. In the background and cylinder domains, material constants are allowed to be negative valued. At the cylinder edges we impose continuity conditions, and between unit cells we impose Bloch-Floquet conditions. This admits the system [15]
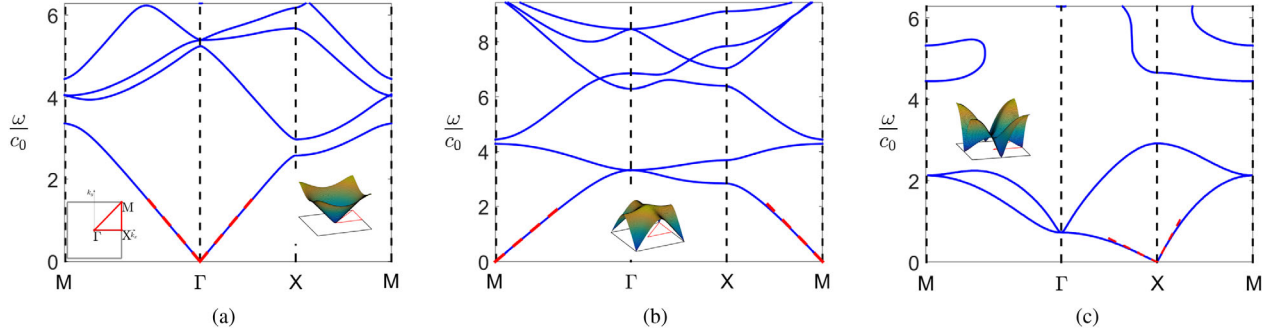
FIG. 1. Band diagrams for square array of cylinders embedded in air with (a) $\varepsilon_c = 1$ and $\mu_c = 2$, (b) $\varepsilon_c = -1$ and $\mu_c = 2$, and (c) $\varepsilon_c \approx -0.53$ and $\mu_c \approx -10.22$. Dashed red lines denote low-frequency descriptions (3), (5), and (8b), respectively. All figures use lattice period $a = 1$, radius $a' = 0.3a$, and dipolar approximation. Inset: first Brillouin zone with path parametrization ΓXM; first band surfaces over first Brillouin zone.

$$N_l \mathcal{B}_l + \sum_{m=-\infty}^{\infty} (-1)^{l+m} S_{m-l}^Y \mathcal{B}_m = 0, \quad (2)$$

where $S_m^Y = S_m^Y(\omega_B, \mathbf{k}_B; n_b)$ denotes lattice sums (see Supplemental Material [16]), $\omega_B = \omega/c_0$, $\mathbf{k}_B = (k_x, k_y)$, $\mathcal{B}_m$ are amplitudes of the cylindrical-harmonic basis functions, and N_m are inverse cylindrical-Mie coefficients. Where applicable, subscripts b and c denote the background and cylinder properties, respectively. The dispersion equation for the crystal is given by the vanishing determinant of (2), which we truncate to dipolar order.

We now outline the procedure for determining when a low-frequency band surface emerges from the Γ point. First, we evaluate expansions for N_m in ω_B (these are lengthy, see Supplemental Material [16]). Next, we determine closed-form expressions for the S_l^Y in (2) at low frequencies and about the Γ point; these are obtained following Chen *et al.* [31] (also extensive, see Supplemental Material [16]). Assuming that $\omega_B = \alpha k_B$, where α is real and positive valued, we subsequently obtain series coefficients for S_l^Y in ω_B alone. Substituting the expansions for N_m and S_l^Y into (2), the zero determinant condition is satisfied to the lowest order for α such that

$$\omega_B = \left\{ \frac{1}{\varepsilon_b} \left(\frac{1+f\tau}{1-f\tau} \right) \frac{1}{\mu_b + f(\mu_c - \mu_b)} \right\}^{1/2} k_B, \quad (3)$$

where $\tau = (\varepsilon_b - \varepsilon_c)/(\varepsilon_b + \varepsilon_c)$, $f = \pi a'^2/a^2$ is the filling fraction, a' denotes the radius of the cylinders, and a is the lattice period. Thus, the constituent permittivity and permeability values can be negative, but provided $\alpha > 0$ then a band surface will emerge from Γ. Here, $\alpha = 1/n_{\text{eff}}$ where n_{eff} is the effective refractive index [15].

Next, we determine the conditions and asymptotic behavior of a band that emerges from the M point at low frequencies. As before, we derive asymptotic forms for the S_l^Y sums near M (see Supplemental Material [16]) and assume $\omega_B = \alpha' k_B'$, where α' is real and positive valued,

$\mathbf{k}_B' = \mathbf{k}_B - \mathbf{M}$ and $\mathbf{M} = (\pi/a, \pi/a)$. This assumption yields series coefficients for S_l^Y in ω_B (given in Supplemental Material [16]). Substituting these expansions for S_l^Y and N_m into (2), the zero determinant condition is satisfied to the lowest orders when

$$\varepsilon_c = -\varepsilon_b, \quad (4)$$

and for α' such that

$$\omega_B = \left\{ \frac{1}{8\pi^2} \left| 64\pi^4 e^{4i\theta_B'} + \Gamma(\tfrac{1}{4})^8 \right|^{1/2} \right.$$
$$\left. \times \left[\varepsilon_b \mu_c + 2\varepsilon_b \mu_b \log\left(\frac{16\pi^2}{f\Gamma(\tfrac{1}{4})^4} \right) \right]^{-1/2} \right\} k_B', \quad (5)$$

where $\Gamma(z)$ is the Gamma function. That is, a band surface is supported from M at low frequencies provided (4) and $\alpha' > 0$ are satisfied. The condition $\varepsilon_c = -\varepsilon_b$ corresponds to an *anomalous resonance* in quasistatic problems [32,33] (discussed below).

Likewise, for the X point at low frequencies, having derived asymptotic forms for the S_l^Y sums near X (see Supplemental Material [16]) we assume that $\omega_B = \alpha'' k_B''$, where α'' is real and positive valued, $\mathbf{k}_B'' = \mathbf{k}_B - \mathbf{X}$, and $\mathbf{X} = (\pi/a, 0)$. Substituting the resulting expansions for S_l^Y, and N_m, into (2), the zero determinant condition is satisfied to leading order when

$$\varepsilon_c = \left(\frac{\zeta - 16\pi^2}{\zeta + 16\pi^2} \right) \varepsilon_b, \quad (6)$$

where $\zeta = \Gamma(\tfrac{1}{4})^4 f$. At the next order, provided

$$\mu_c = \left(\frac{\zeta(\zeta - 64\pi^2) + 512\pi^4 \log\left[\zeta/(32\pi^2)\right]}{(\zeta - 16\pi^2)^2} \right) \mu_b, \quad (7)$$

then we obtain the low-frequency dispersion relation
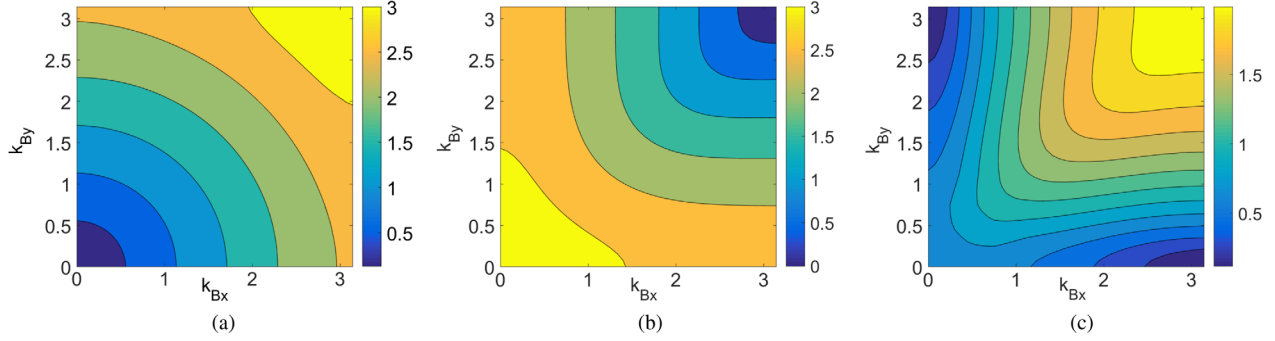
FIG. 2.   Isofrequency contours of first band surface ω/c_0 for configurations in Fig. 1.

$$\omega_B = \left\{ \frac{[16\Gamma(\tfrac{1}{4})^4\pi^2 + 64\pi^4 e^{2i\theta_B''} - \Gamma(\tfrac{1}{4})^8 e^{-2i\theta_B''}]}{16\Gamma(\tfrac{1}{4})^4\pi^2\varepsilon_b\mu_b} \right\}^{1/2} k_B''.$$

(8a)

However, the slope in (8a) is only real valued along ΓX and XM. Numerical investigations confirm elliptical contours at low frequencies; interpolating between these paths with the ansatz $\omega_B^2 = \alpha_x'' k_{Bx}''^2 + \alpha_y'' k_{By}''^2$ we obtain

$$\omega_B^2 = \left(\frac{16\Gamma(\tfrac{1}{4})^4\pi^2 + 64\pi^4 - \Gamma(\tfrac{1}{4})^8}{16\Gamma(\tfrac{1}{4})^4\pi^2\varepsilon_b\mu_b} \right) k_{Bx}''^2$$
$$+ \left(\frac{16\Gamma(\tfrac{1}{4})^4\pi^2 - 64\pi^4 + \Gamma(\tfrac{1}{4})^8}{16\Gamma(\tfrac{1}{4})^4\pi^2\varepsilon_b\mu_b} \right) k_{By}''^2, \quad (8b)$$

for the first band surface as $\omega_B \to 0$ and as $\mathbf{k}_B \to X$. Hence, a band surface is supported from X at low frequencies provided (6), (7), and $\varepsilon_b\mu_b > 0$ are satisfied. In (6), the proportionality factor is negative valued for $f \lesssim 0.914$, and the proportionality factor in (7) is negative valued for all f, demonstrating that highly restrictive sign-changing conditions must be satisfied in both ε_r and μ_r so that the first band emerges from X. The number of conditions for each high-symmetry Bloch coordinate is entirely due to the different asymptotic behaviors of S_l^Y. For arbitrary Bloch coordinate origin, we anticipate that the number of conditions will change significantly.

We now compare the asymptotic forms above against results from a fully numerical treatment of (2) within the dipole truncation. We begin by validating (3) for a regular photonic crystal; in Fig. 1(a) we present the band diagram of a representative crystal with $\varepsilon_c = 1$ and $\mu_c = 2$ embedded in air ($\varepsilon_b = \mu_c = 1$). As expected, the first band emanates from the Γ point, and (3) shows excellent agreement. In Fig. 1(b) we consider $\varepsilon_c = -1$ and $\mu_c = 2$, where the first band emanates from the M point as described by (5) at low frequencies, also with excellent agreement. In Fig. 1(c) we consider $\varepsilon_c \approx -0.53$ and $\mu_c \approx -10.22$ satisfying (6) and (7). Here, the slope differs along ΓX and XM, demonstrating twofold symmetry as $\omega_B \to 0$. The asymptotic estimate (8a) shows excellent agreement

near X at low frequencies. The diagram also possesses folded bands [9] at high frequencies.

In Fig. 2 we present isofrequency contours for the first band surfaces of the photonic crystals considered in Fig. 1, over a quarter of the first Brillouin zone. In Fig. 2(a) we see a cone (∞ symmetric) as $\omega_B \to 0$, whereas in Fig. 2(b) we observe fourfold symmetric contours, as expected from the $\exp(4i\theta_B')$ dependence in (5). In Fig. 2(c) we see that the first band has twofold symmetric contours, as expected from (8b). These low-frequency symmetries contrast with the electronic band diagrams of graphene (and photonic analogues to graphene) where the high-energy band emanates from the K point and about the Fermi energy E_F as an ideal cone [34–36].

Having numerically validated the $E - k$ relations (3), (5), and (8), we now briefly demonstrate that magnetic constituents are not necessary to observe exotic low-frequency behaviors. Low-frequency descriptions of nonmagnetic photonic crystals emanating from Γ and M are obtained by the replacements $\mu_b, \mu_c \mapsto 1$ in (3) and (5) above. This is despite the fact that the N_m coefficients for nonmagnetic crystals exhibit different leading order behavior for small ω_B (see Supplemental Material [16]). However, the new leading-order behavior of N_m yields a nonmagnetic analogue to (7) of the form

$$\zeta + 8\pi^2 - 16\pi^2 \log\left[\zeta/(32\pi^2)\right] = 0, \quad (9)$$

which is not satisfied for any f. As such, low-frequency emanation from X as $\omega_B = \alpha'' k_B''$ or $\omega_B^2 = \alpha_x'' k_{Bx}''^2 + \alpha_y'' k_{By}''^2$ is not supported for nonmagnetic crystals.

In Fig. 3 we present first band(s) for a selection of crystals comprising nonmagnetic cylinders ($\mu_c = 1$) in air, and describe their evolution as ε_c is varied from $0 < \varepsilon_c \le -2.1$. For values $0 > \varepsilon_c \gtrsim -0.5274$ (6), a single first band emanates from the Γ point, analogously to the Γ-emerging band in Fig. 3(a). At $\varepsilon_c \approx -0.5274$, a band emerges from the X point, giving rise to two first band surfaces at low frequencies, as in Fig. 3(a). This X-emergent surface eventually forms a double degeneracy at the Γ point at $\varepsilon_c \approx -0.56$, and thereafter, as shown in Fig. 3(b), becomes
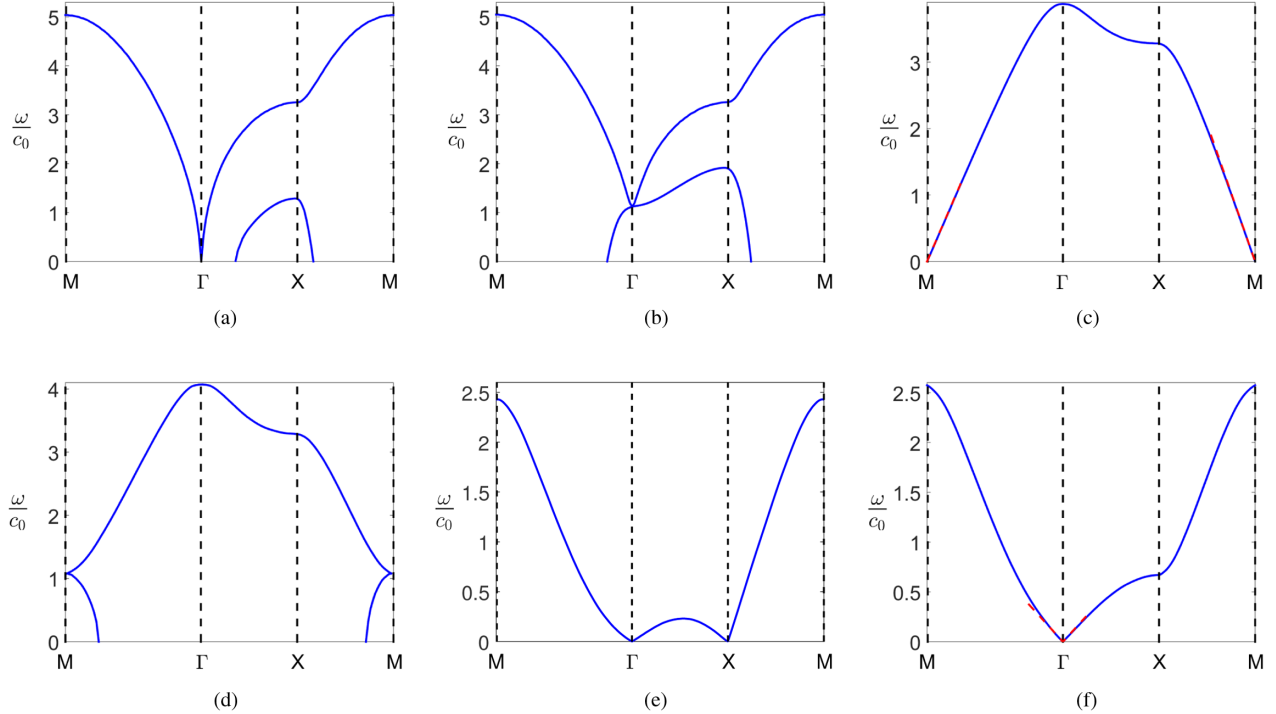
FIG. 3.   Band diagrams for square array of nonmagnetic cylinders ($\mu_c = 1$) embedded in air ($\varepsilon_b = \mu_b = 1$) with (a) $\varepsilon_c = -0.55$, (b) $\varepsilon_c = -0.58$, (c) $\varepsilon_c = -1$, (d) $\varepsilon_c = -1.1$, (e) $\varepsilon_c \approx -1.896$, and (f) $\varepsilon_c = -2.1$. Dashed red lines in (c) and (f) are approximations (5) and (3), respectively. All figures use a dipolar approximation, lattice period $a = 1$, and radius $a' = 0.3a$.

the first band surface, pushing the existing Γ centered band to higher frequencies. As we proceed in ε_c, the origin of the first band travels along the ΓM and ΓX symmetry planes to the M point at $\varepsilon_c = -1$ (the anomalous resonance condition), as shown in Fig. 3(c). Thereafter, a new first band emerges at the M point whose origins move along high symmetry planes towards the Γ point. At the same time, this emergent band pushes the existing M centered band to higher frequencies. Both of these behaviors are demonstrated in Fig. 3(d). The new first band eventually takes the form given in Fig. 3(e) where it emanates from both the Γ and X points simultaneously at $\varepsilon_c = (\zeta + 16\pi^2)/(\zeta - 16\pi^2) \approx -1.896$. As we proceed in ε_c, the first eigenfrequency at X becomes nonzero and the first band emanates from the Γ point alone, as demonstrated by Fig. 3(f). Undoubtedly further behaviors are observed beyond $\varepsilon_b < -2.1$; however, this falls outside the scope of the present work. Note that in Figs. 3(c) and 3(f) the dipolar approximations (5) and (3) are superposed, respectively, and show excellent agreement at low frequencies. The examples above, in consideration with (9), emphasize that the absence of a band from a single Bloch coordinate does not preclude the emergence of bands from multiple Bloch coordinates simultaneously; this observation has important implications for determining the existence of band gaps at low frequencies. We emphasize that the band structure smoothly transitions between the examples shown above.

In summary, we have determined new low-frequency $E - k$ relations for photons in 2D photonic crystals. These relations, and the conditions for their existence, are given explicitly for first bands with origins at the Γ, X, and M points of a square lattice. In general, we have found that sign changes in the properties of the constituents are required for the first band to originate from coordinates away from Γ at low frequencies. We have also demonstrated that photonic crystals can possess low-frequency $E - k$ relations with origins at one or more arbitrary Bloch coordinates. Given that all conventional photonic crystals possess either a low-frequency band gap or a band surface emanating from Γ, this work has significant implications for the homogenization of periodic media, theoretical descriptions of light propagation in complex media, as well as future photonic crystal designs. In the latter case, the closed-form conditions we obtain represent a powerful design tool for determining filling fractions and background materials for a given cylinder material, and vice versa. However, an important consequence of the M-point condition coinciding with the anomalous resonance condition is that the slope of the M-emerging band (5) is not necessarily accurate beyond a dipolar truncation; further investigations are required to accurately determine behaviors near resonance (see Supplemental Material [16]). Preliminary results for hexagonal lattices at the anomalous resonance reveal a band surface emerging from the K point, implying that the first band originates from the furthest edge of the irreducible Brillouin zone when on resonance. Away from the anomalous resonance condition, we believe

that experimental validation is feasible for the crystals we describe, as all emergence conditions [i.e., (6) and (7)] are valid for complex-valued ε_b and μ_b. When ε_b and μ_b possess moderate loss, and ε_c and μ_c satisfy the necessary emergence conditions, we find the band diagrams to be unchanged (see Supplemental Material [16]). A natural next step for this work is 1D and 3D photonic structures; 2D photonic crystals were only chosen for analytical convenience. Finally, we emphasize that our approach extends readily to phononic and other systems.

---

*michael.j.smith@manchester.ac.uk

[1] J. D. Joannopoulos, S. G. Johnson, J. N. Winn, and R. D. Meade, *Photonic Crystals: Molding the Flow of Light* (Princeton University Press, Princeton, 2008).

[2] M. Born and E. Wolf, *Principles of Optics: Electromagnetic Theory of Propagation, Interference and Diffraction of Light* (Pergamon Press, New York, 1964).

[3] C. Kittel, *Introduction to Solid State Physics* (John Wiley & Sons, New York, 2005).

[4] D. R. Smith, J. B. Pendry, and M. C. K. Wiltshire, Science **305**, 788 (2004).

[5] V. G. Veselago, Sov. Phys. Usp. **10**, 509 (1968).

[6] J. B. Pendry, Phys. Rev. Lett. **85**, 3966 (2000).

[7] S. Fan, P. R. Villeneuve, and J. D. Joannopoulos, Phys. Rev. B **54**, 11245 (1996).

[8] G. Lerario, A. Fieramosca, F. Barachati, D. Ballarini, K. S. Daskalakis, L. Dominici, M. De Giorgi, S. A. Maier, G. Gigli, S. Kéna-Cohen *et al.*, Nat. Phys. **13**, 837 (2017).

[9] P. Y. Chen, C. G. Poulton, A. A. Asatryan, M. J. Steel, L. C. Botten, C. M. de Sterke, and R. C. McPhedran, New J. Phys. **13**, 053007 (2011).

[10] S. Guenneau, S. Anatha Ramakrishna, S. Enoch, S. Chakrabarti, G. Tayeb, and B. Gralak, Photonics Nanostruct. Fundam. Appl. **5**, 63 (2007).

[11] J. Helsing, R. C. McPhedran, and G. W. Milton, New J. Phys. **13**, 115005 (2011).

[12] J. Li, L. Zhou, C. T. Chan, and P. Sheng, Phys. Rev. Lett. **90**, 083901 (2003).

[13] W. A. Harrison, *Electronic Structure and the Properties of Solids: The Physics of the Chemical Bond* (Dover, New York, 1989).

[14] F. Cora, M. Stachiotti, C. Catlow, and C. Rodriguez, J. Phys. Chem. B **101**, 3945 (1997).

[15] A. B. Movchan, N. V. Movchan, and C. G. Poulton, *Asymptotic Models of Fields in Dilute and Densely Packed Composites* (Imperial College Press, London, 2002).

[16] See Supplemental Material at http://link.aps.org/supplemental/10.1103/PhysRevLett.121.103902 for definitions of lattice sums, derivations of asymptotic forms, and detailed discussions, which includes Refs. [17–30].

[17] R. C. McPhedran, C. G. Poulton, N. A. Nicorovici, and A. B. Movchan, Proc. R. Soc. A **452**, 2231 (1996).

[18] C. G. Poulton, A. B. Movchan, R. C. McPhedran, N. A. Nicorovici, and Y. A. Antipov, Proc. R. Soc. A **456**, 2543 (2000).

[19] R. C. McPhedran, N. P. Nicorovici, L. C. Botten, and K. A. Grubits, J. Math. Phys. (N.Y.) **41**, 7808 (2000).

[20] C. M. Linton, J. Eng. Math. **33**, 377 (1998).

[21] V. Twersky, Arch. Ration. Mech. Anal. **8**, 323 (1961).

[22] S. K. Chin, N. A. Nicorovici, and R. C. McPhedran, Phys. Rev. E **49**, 4590 (1994).

[23] A. Bensoussan, J. L. Lions, and G. Papanicolaou, *Asymptotic Analysis for Periodic Structures* (North-Holland Publishing Company, Amsterdam, 1978).

[24] V. V. Jikov, S. M. Kozlov, and O. A. Oleinik, *Homogenization of Differential Operators and Integral Functionals* (Springer-Verlag, Berlin, 1994).

[25] D. J. Bergman, J. Phys. C **12**, 4947 (1979).

[26] R. C. McPhedran and D. R. McKenzie, J. Appl. Phys. **23**, 223 (1980).

[27] K. Busch and S. John, Phys. Rev. E **58**, 3896 (1998).

[28] C. M. Linton, SIAM Rev. **52**, 630 (2010).

[29] M. Abramowitz and I. A. Stegun, *Handbook of Mathematical Functions with Formulas, Graphs, and Mathematical Tables* (Dover Publications, New York, 1972).

[30] N. A. Nicorovici, C. G. Poulton, and R. C. McPhedran, J. Math. Phys. (N.Y.) **37**, 2043 (1996).

[31] P. Y. Chen, M. J. A. Smith, and R. C. McPhedran, J. Math. Phys. (N.Y.) **59**, 072902 (2018).

[32] N. A. Nicorovici, R. C. McPhedran, and G. W. Milton, Phys. Rev. B **49**, 8479 (1994).

[33] N. A. Nicorovici, G. W. Milton, R. C. McPhedran, and L. C. Botten, Opt. Express **15**, 6314 (2007).

[34] S. Reich, J. Maultzsch, C. Thomsen, and P. Ordejon, Phys. Rev. B **66**, 035412 (2002).

[35] Y. Zhang, Y.-W. Tan, H. L. Stormer, and P. Kim, Nature (London) **438**, 201 (2005).

[36] S. R. Zandbergen and M. J. A. de Dood, Phys. Rev. Lett. **104**, 043903 (2010).